Drag enhancement in a dusty Kolmogorov flow

Drag enhancement in a dusty Kolmogorov flow

A. Sozza,[1,*] M. Cencini,[1,†] S. Musacchio,[2] and G. Boffetta[2]

[1] *Istituto dei Sistemi Complessi, CNR and INFN sez. Roma2 "Tor Vergata", via dei Taurini 19, 00185 Rome, Italy.*

[2] *Dipartimento di Fisica and INFN, Universitá di Torino, via P. Giuria 1, 10125 Torino, Italy.*

Particles suspended in a fluid exert feedback forces that can significantly impact the flow, altering the turbulent drag and velocity fluctuations. We study flow modulation induced by small spherical particles heavier than the carrier fluid in the framework of an Eulerian two-way coupled model, where particles are represented by a continuum density transported by a compressible velocity field, exchanging momentum with the fluid phase. We implement the model in direct numerical simulations of the turbulent Kolmogorov flow, a simplified setting allowing for studying the momentum balance and the turbulent drag in the absence of boundaries. We show that the amplitude of the mean flow and the turbulence intensity are reduced by increasing particle mass loading with the consequent enhancement of the friction coefficient. Surprisingly, turbulence suppression is stronger for particles of smaller inertia. We understand such a result by mapping the equations for dusty flow, in the limit of vanishing inertia, to a Newtonian flow with an effective forcing reduced by the increase in fluid density due to the presence of particles. We also discuss the negative feedback produced by turbophoresis which mitigates the effects of particles, especially with larger inertia, on the turbulent flow.

* Corresponding author; asozza.ph@gmail.com

† Corresponding author; massimo.cencini@cnr.it

I. INTRODUCTION

Dust and particulate in turbulent flows are common to many natural environments [1], from aerosol in clouds formation [2, 3], particle-driven gravity currents [4], sediment transport in rivers [5], and volcanic eruptions [6], to planetesimals and proto-planets formation [7–9]. They are also relevant to many industrial processes dealing with pipe flows and open channel flows [10], as well as in fluidization processes [11].

Dispersed particles are not only transported by the flow, but they exert forces (e.g. drag forces) on the fluid that, depending on the mass loading, can modify the flow itself. The coupled system made of the carrier fluid and the particles is generally referred to as particle-laden flow [12]. The interactions between the particles and the fluid can significantly alter the flow both at large and small scales. In particular, heavy particles can attenuate or enhance turbulence depending on their size with respect to the viscous scale [12, 13]. In general, smaller [14, 15] and settling [16–18] particles lead to turbulence attenuation. Less clear is the effect on turbulent drag: experiments in channel flows did not find measurable changes on the mean flow [14, 15], while simulations reported drag reduction in a channel flow [19] and drag enhancement in an unstably stratified boundary layer [20], moreover the effects depend sensitively on many factors including particle shape, size and volume/mass fraction [21, 22]. At small scales, effects of particles on the carrier fluid have been observed in the spectral distribution of the fluid kinetic energy [23–25].

Turbulence in multiphase flows constitutes a formidable challenge even in the dilute regime, where the fluid-particle interactions causes also the formation of strong inhomogeneities in particles' spatial distribution [12]. Fractal clustering of (one-way coupled) particles has been observed at small scales in chaotic flows [26, 27] and within the inertial and dissipative range of turbulence [28]. In inhomogeneous turbulent flows large-scale clustering of particle occurs because of the turbophoresis, that is, the migration of the particles in regions of lower turbulence intensity [29, 30]. Due to its importance for applications, turbophoresis is usually studied in the presence of boundaries, such as in turbulent boundary layers [31–35], pipe flows [36] and channel flows [37]. Nevertheless, turbophoresis does not require the presence of boundaries, but just the spatial modulation of the turbulent intensity, and has been observed also in the absence of walls [38–40].

In this paper, we investigate the effects of mass loading and particle inertia on turbulent drag and turbophoresis in bulk flows without material boundaries, in the regime of low volume fraction. To this aim we have performed numerical simulations of a two-way coupled fully Eulerian model, first introduced by Saffman [41], for a dilute suspension of inertial particles in a turbu-

lent Kolmogorov flow. The Kolmogorov flow is obtained by forcing the Navier-Stokes equations with a sinusoidal force, and was originally proposed by Kolmogorov as a model to understand the transition to turbulence [42]. It represents a paradigm of inhomogeneous turbulent flows without boundaries, because the local intensity of turbulent fluctuations is spatially modulated by the presence of a sinusoidal mean velocity profile. Owing to the spatial variation of the turbulent intensity, the Kolmogorov flow provides an ideal setup to study the turbophoretic effect in the absence of boundaries [39, 43]. Furthermore, the presence of a mean flow allows us to define a drag (or friction) coefficient, as the ratio between the work made by the force and the kinetic energy carried by the mean flow [44]. In this regard, the Kolmogorov flow can be thought of as a simplified channel flow without boundaries, and it has been exploited for numerical studies of the bulk processes of drag reduction in dilute polymer solutions [45], drag enhancement in dilute solutions of inextensible rods [46] and in spatially fixed networks of rigid fibers [47].

We find that particles modify the bulk properties of the flow by reducing the amplitude of the mean flow and the intensity of turbulent fluctuations, at increasing the mass loading. The reduced mean flow at fixed forcing amplitude implies an increase of the drag coefficient. Surprisingly, we find that this effect is larger for particles with smaller inertia. Turbulence reduction at increasing mass loading also results in a reduction of the turbophoretic effect, in agreement with previous findings in channel flows [48].

The paper is organized as follows. In Sec. II, we describe the Eulerian model for a dusty fluid. In Sec. III, we detail the numerical implementation of the model and report the parameters used in the simulations. In Sec. IV, we present the main results of our study. Finally, in Sec. V we summarize the results and discuss the perspectives of our study. In the Appendix we benchmark the model against previous Lagrangian simulations (in the passive case) and against different regularization scheme for the particle velocity and density fields.

II. EULERIAN MODEL FOR A DUSTY FLUID

Theoretical and numerical studies of particle laden flows make use of different models to describe the interactions between particles and fluid [12], based either on Eulerian-Lagrangian approaches (see, e.g., Refs. [23, 25]) or Eulerian two-phase models (e.g., Refs. [24, 41]). Here we adopt an Eulerian model with two-way coupling appropriate for suspensions with negligible volume fraction, which was first introduced by Saffman to study the linear stability of a dusty gas [41].

The Saffman model has been used in astrophysical studies, and in particular to describe the

dynamics of protoplanetary disks [8]. Within this context, the coupling between the gas and particle phases in a rotating Keplerian disk leads to the streaming instability [49] which is one hypothesis for planetesimal formation, overcoming the small scale bottleneck of self-gravitation [50].

We consider a dilute mono-disperse suspension of small, heavy, spherical particles with density ρ_p and size a transported in a Newtonian fluid with density ρ_f and viscosity μ. The particle density is assumed to be much larger than fluid one, $\rho_p \gg \rho_f$. In real systems, the density ratio ρ_p/ρ_f can easily reach order 10^3 for grains or water droplets in air and order 10 for metallic particles in water. We assume the particle size much smaller than the viscous scale of the flow, $a \ll \eta$, where $\eta = (\nu^3/\varepsilon)^{1/4}$ is the Kolmogorov viscous length and ε the fluid kinetic energy dissipation rate. This assumption implies that the particle Reynolds number is small and we further assume that the volume fraction of the particles $\Phi_v = N_p v_p/V$, defined in terms of the volume of each particle $v_p \propto a^3$ and the number of particles N_p contained in the total volume V, is negligible small. Even for very small volume fraction, the mass loading $\Phi_m = \Phi_v \rho_p/\rho_f$ can be of order unity because of the large density ratio. As an example, for a dilute suspension of droplets of water in air with $\Phi_v \approx 10^{-3}$ one has $\Phi_m \approx 1$.

Because of the vanishing volume fraction of the particles, the fluid density field can be assumed to be constant and, therefore, the velocity field of the fluid phase $\boldsymbol{u}(\boldsymbol{x}, t)$ incompressible ($\boldsymbol{\nabla} \cdot \boldsymbol{u} = 0$). The solid phase is described by the particles' velocity field $\boldsymbol{v}(\boldsymbol{x}, t)$ and the normalized number density field $\theta(\boldsymbol{x}, t) = n(\boldsymbol{x}, t)/(N_p/V)$, where $n(\boldsymbol{x}, t)$ is the local number of particles per unit volume. The normalization gives $\langle \theta \rangle = 1$. Here and in the following, the brackets $\langle [\cdot] \rangle$ denote the average over the whole volume V.

For small volume fractions ($\Phi_v < 10^{-3}$) the dynamics of the particle-laden flow can be described by a two-way coupling, which takes into account the interactions between individual particles and the surrounding flow, but neglects the interactions between particles (collisions and friction) and the particle-fluid-particle interactions (fluid streamlines compressed between particles) [51]. In the two-way coupling regime, the exchange of momentum between the two phases can no longer be neglected [12]. For small heavy particles, such an exchange is mainly mediated by the viscous drag force $\boldsymbol{f}_{drag} = \gamma(\boldsymbol{v} - \boldsymbol{u})$, which is proportional to the velocity difference between particle and fluid velocity, γ being the viscous drag coefficient.

Assuming that the interactions conserve the total momentum, Saffman [41] derived the following

coupled equations for the two phases:

$$\partial_t \boldsymbol{u} + \boldsymbol{u}\cdot\boldsymbol{\nabla}\boldsymbol{u} = -\frac{\boldsymbol{\nabla} p}{\rho_f} + \nu\boldsymbol{\nabla}^2\boldsymbol{u} + \boldsymbol{f}_{ext} + \frac{\Phi_m}{\tau}\theta(\boldsymbol{v}-\boldsymbol{u}) \tag{1}$$

$$\partial_t \boldsymbol{v} + \boldsymbol{v}\cdot\boldsymbol{\nabla}\boldsymbol{v} \ = -\frac{\boldsymbol{v}-\boldsymbol{u}}{\tau} \tag{2}$$

$$\partial_t \theta + \boldsymbol{\nabla}\cdot(\boldsymbol{v}\theta) = 0\,, \tag{3}$$

where p is the pressure, $\boldsymbol{f}_{ext}$ is the external force, which sustains the flow, $\nu = \mu/\rho_f$ is the kinematic viscosity, and $\tau = m_p/\gamma$ is the particle relaxation time, defined as the ratio between the particle mass $m_p = \rho_p v_p$ and its viscous drag coefficient γ. In the case of a spherical particles of radius a one has $m_p = (4/3)\pi a^3\rho_p$ and $\gamma = 6\pi\mu a$, which gives the Stokes time $\tau = (2/9)a^2\rho_p/\rho_f\nu$. Normalizing the latter with the Kolmogorov viscous time, $\tau_\eta = (\nu/\varepsilon)^{1/2}$, we obtain the Stokes number $St = \tau/\tau_\eta$, which provides a non-dimensional measure of particle inertia in responding to the fluid velocity fluctuations.

It is important to remark that the validity of the model (1-3) is limited to small Stokes numbers $St < 1$. In a Lagrangian description, nearby particles with large St may exhibit very different velocities [52], a phenomenon known under the name of caustics formation [53] and sling effect [54]. Within the Eulerian framework, caustics would imply a multi-valued particle velocity field, breaking the validity of the continuum description. The rate of caustic formation increases with St [55], therefore the Eulerian description for the particles is valid only for sufficiently small inertia, when the effect of caustics is negligible. A direct comparison of the model (1-3) (for $\Phi_m = 0$) with Lagrangian simulations has shown that the Eulerian and Lagrangian approaches are equivalent for $St < 1$ [56]. Moreover, in Eq. (2) we have neglected the gravity acceleration $\boldsymbol{g}$ on the particles to avoid additional effects induced by sedimentation.

Noticing that in the case of spherical particles the Stokes number can be written as $St = (2/9)(\rho_p/\rho_f)(a/\eta)^2$, it is easy to realize that the condition $St < 1$ for the validity of the Eulerian description can be fulfilled only by very small particles with $a \ll \eta$. In order to obtain finite values for the parameters τ and Φ_m, the limit of vanishing radius $a \to 0$ can be consistently achieved in the model (1-3) by assuming the scaling $\rho_p/\rho_f \sim a^{-2}$ for the density ratio and $N_p \sim a^{-1}$ for total number of particles. These scalings ensure the volume fraction to vanish as $\Phi_v \sim a^2$.

We also remark that the two-way coupling used in the above model does not preserve the total kinetic energy of the fluid and particle phases. Defining the kinetic energy per unit volume as $E = \rho_f(\langle|\boldsymbol{u}|^2\rangle + \Phi_m\langle\theta|\boldsymbol{v}|^2\rangle)/2$ the energy balance of the model is:

$$\frac{dE}{dt} = \rho_f\left[-\nu\langle(\boldsymbol{\nabla}\boldsymbol{u})^2\rangle - \frac{\Phi_m}{\tau}\langle\theta|\boldsymbol{v}-\boldsymbol{u}|^2\rangle + \langle\boldsymbol{f}_{ext}\cdot\boldsymbol{u}\rangle\right]\,, \tag{4}$$

which shows that a fraction of the energy injected by the external force is removed by the viscous drag between the particles and the fluid.

In this paper, as for the external force stirring the fluid, we consider the Kolmogorov force $\boldsymbol{f}_{ext} = F\cos(Kz)\hat{\boldsymbol{x}}$. Under this forcing one has a simple laminar solutions to (1-3) given by $\theta = 1$ and $\boldsymbol{u} = \boldsymbol{v} = U_0\cos(Kz)\hat{\boldsymbol{x}}$ with $U_0 = F/(\nu K^2)$. In the absence of particles ($\Phi_m = 0$), this solution becomes unstable to transverse large-scale perturbations (for wavenumber smaller than K) when the Reynolds number $\mathrm{Re} = U_0/(\nu K)$ exceeds the critical threshold $\mathrm{Re}_c = \sqrt{2}$ [57]. Remarkably, even in the turbulent regime, the Kolmogorov flow maintains a monochromatic mean velocity profile $\overline{\boldsymbol{u}} = U\cos(Kz)\hat{\boldsymbol{x}}$ with an amplitude U smaller than the laminar solution U_0 (here and in the following the over-bar $\overline{[\cdot]}$ denotes the average over time t and over the x and y coordinates). The presence of a non-vanishing mean velocity profile allows us to define the turbulent drag coefficient [44] $f = F/(KU^2)$, in analogy with channel flows.

In summary, the dimensionless parameters which control the dynamics of the model are the mass loading $\Phi_m = \Phi_v\rho_p/\rho_f$, the Reynolds number $Re = U/(\nu K)$, defined in terms of the amplitude U of the turbulent mean profile of the x-component of the velocity, and the Stokes number $St = \tau/\tau_\eta$.

III. NUMERICAL SIMULATIONS

We performed numerical simulations of Eqs. (1-3) by means of a 2/3 de-aliased pseudo-spectral solver with second-order Runge-Kutta time marching in a triply periodic cubic domain of side $L = 2\pi$ and grid resolution $M = 256$. Small scale resolution of the fields was ensured by requiring $k_{max}\eta \geq 2.7$ ($k_{max} = M/3$). We explored three values of Stokes time $\tau = (0.10, 0.34, 0.58)$ and three values of mass loading $\Phi_m = (0.0, 0.4, 1.0)$, which compose a dataset of nine configurations in the parameters space. The simulations with $\Phi_m = 0$ correspond to the case with passive inertial particles, previously studied in Ref. [39] using a Lagrangian scheme, whose results were used to benchmark the Eulerian model (see Appendix A 1). We notice that the values of dimensionless parameters Re and St depends also on the mass loading Φ_m and are therefore determined *a posteriori* in the simulations. The main parameters of our simulations are summarized in Table I.

In each run we let the simulations evolve to reach a statistically stationary state, discarding transient behaviors. The particles were initialized with a homogeneous density field ($\theta = 1$) and velocity field equal to the fluid one ($\boldsymbol{v} = \boldsymbol{u}$). After the transient, we collected 360 profiles and fields, over a temporal series of 500 eddy turnover time, in order to ensure statistical convergence. The statistical uncertainties (represented by the error-bars in the figures) have been estimated using the

Run	τ	Φ_m	U	A	u'_{rms}	B	θ'_{rms}	ε	τ_η	Re	St	R_λ
A1	0.10	0.0	0.232	0.020	0.199	6.53×10^{-3}	0.264	9.3×10^{-4}	1.04	232	0.10	89
A2	0.10	0.4	0.195	0.016	0.164	4.29×10^{-3}	0.185	4.8×10^{-4}	1.44	195	0.07	85
A3	0.10	1.0	0.160	0.012	0.134	2.97×10^{-3}	0.133	2.7×10^{-4}	1.93	160	0.05	76
B1	0.34	0.0	0.233	0.047	0.199	6.62×10^{-3}	0.634	9.3×10^{-4}	1.04	233	0.33	89
B2	0.34	0.4	0.197	0.039	0.160	4.34×10^{-3}	0.444	4.2×10^{-4}	1.54	197	0.22	89
B3	0.34	1.0	0.169	0.030	0.131	3.02×10^{-3}	0.324	2.4×10^{-4}	2.06	169	0.17	83
C1	0.58	0.0	0.233	0.061	0.199	6.68×10^{-3}	0.922	9.3×10^{-4}	1.04	233	0.56	89
C2	0.58	0.4	0.200	0.048	0.158	4.59×10^{-3}	0.634	4.0×10^{-4}	1.058	200	0.37	92
C3	0.58	1.0	0.174	0.038	0.129	3.18×10^{-3}	0.458	2.2×10^{-4}	2.12	174	0.27	87

TABLE I. Simulation parameters: Run index, Stokes time τ, mass loading Φ_m, amplitude of the mean flow U, amplitude of the modulation of the particle density profile A, Root mean square (RMS) velocity fluctuations u'_{rms}, amplitude of the modulation of the profile of square velocity fluctuations B, RMS particle density fluctuations θ'_{rms}, energy dissipation rate $\varepsilon = \nu\langle(\boldsymbol{\nabla u})^2\rangle$, Kolmogorov time $\tau_\eta = (\nu/\varepsilon)^{1/2}$, Reynolds number $Re = U/(K\nu)$, Stokes number $St = \tau/\tau_\eta$, Taylor-scale Reynolds number $R_\lambda = \langle|\boldsymbol{u}|^2\rangle\sqrt{5/(3\nu\varepsilon)}$. In all runs we used resolution $M = 256$, kinematic viscosity $\nu = 10^{-3}$, forcing amplitude $F = 8 \times 10^{-3}$, forcing wave-number $K = 1$.

variations observed by halving the statistics. In order to avoid the development of instabilities due to strong density gradients, which are unavoidable due to particle clustering, we added a numerical regularization to Eqs. (2-3). In particular, we considered an additional viscous term $\nu_p\nabla^2\boldsymbol{v}$ and diffusivity $\kappa_p\nabla^2\theta$ for the particle velocity and density field, respectively. To reduce the number of parameters, we fixed $\nu_p = \kappa_p = \nu$. To check the robustness of our results with respect to the regularization scheme, we performed additional simulations with an alternative regularization based on higher-order Laplacian. In Appendix A 2 we compare the results obtained with the two methods.

Finally, we observe that in principle the pseudo-spectral scheme does not preserve the positivity of the density field. Indeed, in low density regions steep gradients and fluctuations of density may occasionally generate events with negative density. Nonetheless we have checked that, even in the worst cases corresponding to small Φ_ms and large τs, the fraction of points with negative density does not exceeds $1 - 2\%$.

IV. RESULTS

We start discussing the numerical results by showing, in Fig. 1, the two-dimensional sections of the particle density field $\theta(x, z)$, and the longitudinal velocity field $u_x(x, z)$ for a given Stokes time $\tau = 0.34$ and different values of the mass loading Φ_m. We notice that the density field is organized in elongated filaments, which are gradually smoothed for increasing mass loading. Moreover, they seem to be disposed parallel to the isolines of the longitudinal velocity u_x, and correlated with regions of strong gradients of the velocity field, where the space between isolines is narrowed. Also the fluctuations of the longitudinal velocity u_x appear to be suppressed with respect to the intensity of the mean flow U at increasing mass loading. Already at a qualitative level, these observations provide a first indication that turbulence in the fluid phase is reduced by the back-reaction of the solid phase.

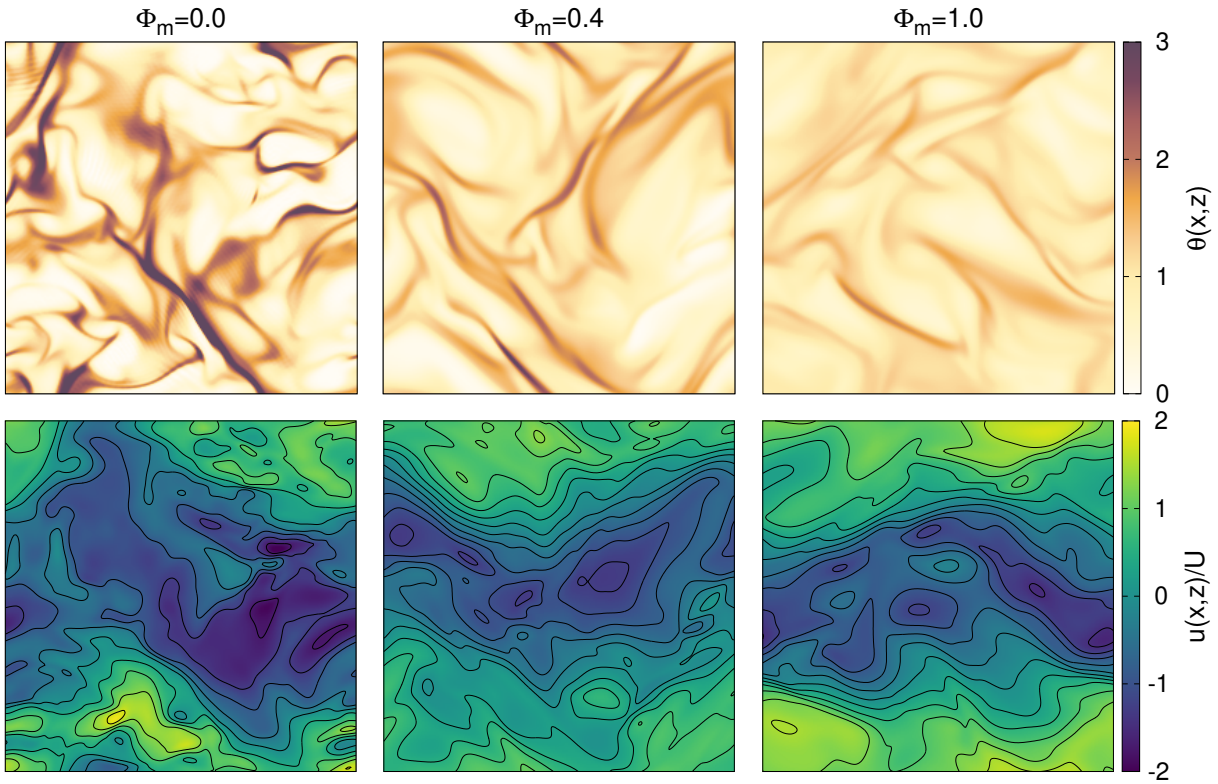

FIG. 1. (Color online) Visualization of two-dimensional sections in the plane (x, z) (at fixed $y = L/2$) of the particle density field θ (top), and longitudinal velocity field u_x (bottom) normalized with the amplitude of the mean flow U. Simulations refer to $\tau = 0.34$ and Φ_m as labeled.

Due to the symmetries of the forcing, which depends on the transverse direction z only, we can define a mean velocity profile $\overline{\boldsymbol{u}}(z)$ by averaging the velocity field $\boldsymbol{u}(x, y, z, t)$ over the coordinates

x, y and time t. Alike the forcing, also the mean velocity profile has non-zero component only in the x-direction: $\overline{\boldsymbol{u}}(z) = (\overline{u}_x(z), 0, 0)$. Furthermore, we decompose the velocity field as the sum of the mean velocity profile and the velocity fluctuations: $\boldsymbol{u} = \overline{\boldsymbol{u}} + \boldsymbol{u}'$.

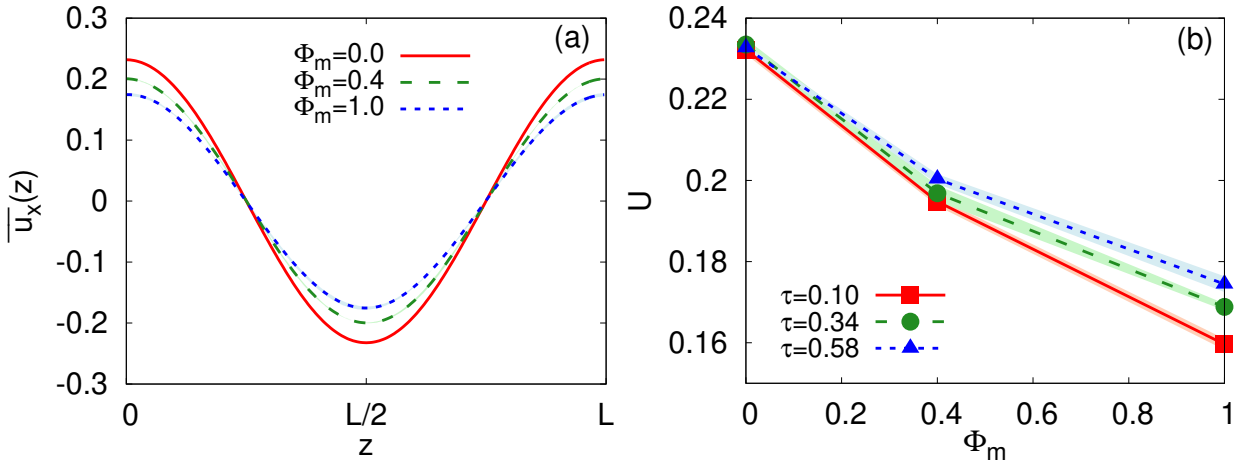

FIG. 2. (Color online) Averaged profiles and amplitudes of the longitudinal fluid velocity. (a) Mean velocity profile $\overline{u_x}(z)$ for different mass loading $\Phi_m = (0.0, 0.4, 1.0)$ and fixed $\tau = 0.58$. (b) Amplitude of the mean flow U as a function of Φ_m for different Stokes time as in label.

In Fig. 2a we show the average profiles of the longitudinal velocity $\overline{u}_x(z)$ for $\tau = 0.58$. Similarly to the case of pure fluid ($\Phi_m = 0$) [44], we find that the profile of the mean flow is, with a good approximation, monochromatic [58]:

$$\overline{u}_x(z) = U \cos(Kz)\,. \tag{5}$$

As shown in Fig. 2b, the amplitude U of the mean velocity profile decreases at increasing the mass loading Φ_m (of about 30% in the case with $\Phi_m = 1$ and $\tau = 0.10$). Even though the dependence of U on τ at fixed Φ_m appears to be milder, Fig. 2b shows that the mean flow is reduced more at smaller τ. In other words, particles with small inertia seem to affect more the mean flow, which is somehow counterintuitive.

The effects of the particles at small St can be explained as follows. When the dust is sufficiently fine, i.e. $\tau \ll \tau_\eta$, particles follow the fluid velocity almost like tracers. From Eq. (2), at the first order in τ one can write $\boldsymbol{v} = \boldsymbol{u} - \tau D_t \boldsymbol{u} + o(\tau)$ [26], where $D_t = \partial_t + \boldsymbol{u} \cdot \boldsymbol{\nabla}$ represents the material derivative. At zero order in τ, the particle velocity field remains incompressible and therefore the particle are homogeneously distributed: $\theta = 1 + O(\tau)$. Substituting the expansions for $\boldsymbol{v}$ and θ in Eq. (1), the equation for the fluid velocity at leading order becomes

$$(1 + \Phi_m) D_t \boldsymbol{u} = -\boldsymbol{\nabla} p + \nu \nabla^2 \boldsymbol{u} + \boldsymbol{f}_{ext}\,. \tag{6}$$

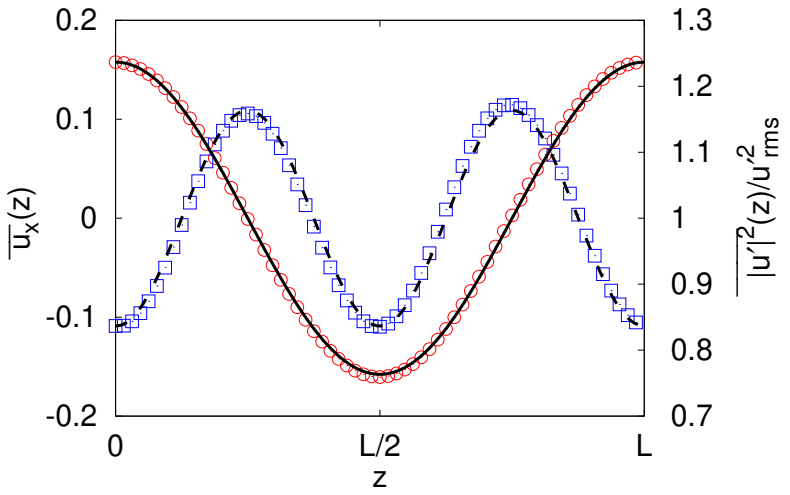

FIG. 3. (Color online) Profiles of the mean longitudinal flow $\overline{u_x}(z)$) (red circles and solid line) and the square velocity fluctuations $\overline{|\boldsymbol{u}'|^2}(z)$ (blue squares and dashed line), for a simulation of the particle-laden flow with $\tau = 0.1$, $\Phi_m = 1.0$ (symbols) and a simulation of a pure fluid with rescaled forcing amplitude $F' = F/(1+\Phi_m)$ (black lines, data from Ref. [44]).

In other terms the fluid density is increased by the presence of particles. At low Reynolds numbers such as in the case of linear stability problems, as previously discussed by Saffman [41], the particle-laden flow is equivalent to a Newtonian fluid with a rescaled viscosity $\nu' = \nu/(1+\Phi_m)$ and therefore particles have a destabilizing effect. Conversely, at high Reynolds numbers, the viscous term is negligible in the momentum budget and the factor $(1+\Phi_m)$ rescales the amplitude of the forcing $\boldsymbol{f}'_{ext} = \boldsymbol{f}_{ext}/(1+\Phi_m)$. According to this argument, one expects that at small St and large Re the main effect of the particles is to cause a reduction of the external forcing and consequently of the mean flow intensity, therefore increasing the turbulent drag. We have tested this prediction by comparing the simulation of the particle-laden flow with $\tau = 0.1$ and $\Phi_m = 1.0$, with a simulation of a pure fluid (i.e., without particles) and rescaled forcing amplitude: $F' = F/(1+\Phi_m)$. As shown in Fig. 3, the profiles of the mean flow $\overline{u}_x(z)$ and of the velocity fluctuations $\overline{|\boldsymbol{u}'|^2}(z)$ obtained in the two cases coincide. We will discuss later the consequences of this effect on the turbulent drag.

Particles impact not only on the mean flow, but also on the turbulent fluctuations $\boldsymbol{u}' = \boldsymbol{u} - \overline{\boldsymbol{u}}$. At increasing mass loading Φ_m, we observe a reduction of the root mean square (RMS) fluid velocity fluctuations $u'_{rms} = \langle |\boldsymbol{u}'|^2 \rangle^{1/2}$ (see Fig. 4a). Actually, fluctuations are suppressed more than the mean flow, as shown by the ratio u'_{rms}/U (inset of Fig. 4a). At fixed Φ_m, the dependence of u'_{rms} on τ is weak (as for U) and it is opposite to what observed for U: particles with smaller τ cause a smaller reduction of u'_{rms}. In the Kolmogorov flow, the intensity of turbulent fluctuations is

not homogeneous. Turbulence is more intense in the regions where the shear of the mean flow is maximum, while it is weaker around the maxima of the mean flow [39, 44]. Therefore, the profile of square velocity fluctuations displays a monochromatic spatial modulation: $\overline{|\boldsymbol{u}'|^2}(z) = (u'_{rms})^2 - B\cos(2Kz)$. As discussed in Ref. [39] (in the case of vanishing mass loading, $\Phi_m = 0$) the amplitude B of the spatial modulation of turbulence intensity is directly related to the turbophoresis. The values of B measured in our simulations are reported in Table I. Alike u'_{rms}, we find that also B is strongly reduced at increasing Φ_m while it weakly depends on τ.

The turbulence attenuation caused by the mass loading reflects into a reduction of the turbophoretic effect. In Fig. 5a we show that the mean particle density profile displays a monochromatic modulation $\overline{\theta}(z) = 1 + A\cos(2Kz)$. Note that the wavelength of the modulation of density is equal to that of the turbulent intensity and it is half that of the mean flow. For $\Phi_m = 0$ the profile obtained is in agreement with the results of the Lagrangian simulations reported in Ref. [39]. The amplitude A of the spatial modulation of the mean density profile provides a quantitative measure of the turbophoretic effect. The values of A are reported in Table I and shown in Fig. 5b. We find that A reduces at increasing the mass loading Φ_m. This effect is directly connected with the reduction of the amplitude B of the variations of the turbulent diffusivity at increasing Φ_m. Furthermore, the amplitude A increases as a function of St collapsing on a master curve for all the values of Φ_m. These results shows that the coupling between the particles and the fluid causes a reduction of the turbophoresis in the Kolmogorov flow, in agreement with what observed in channel flows [48].

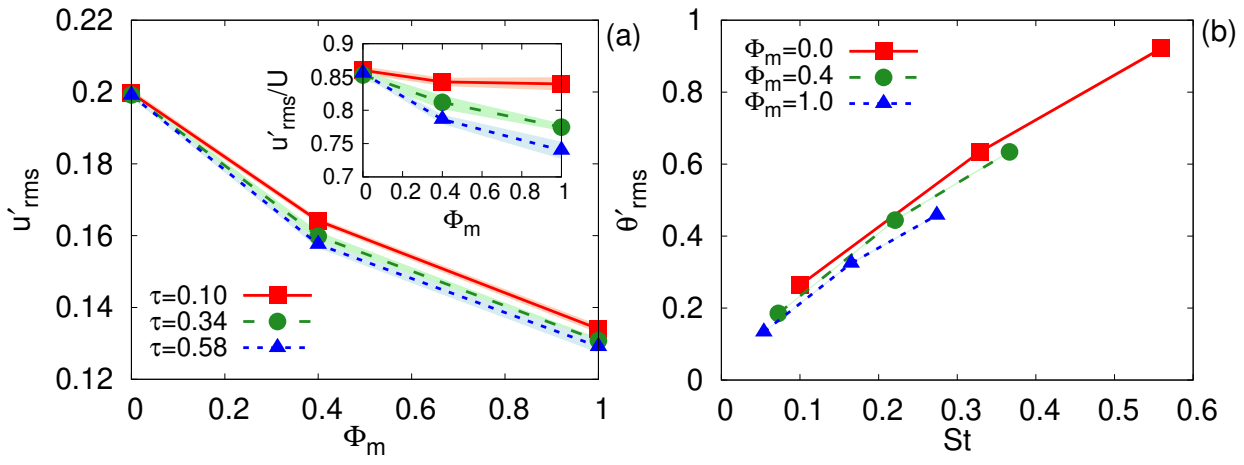

FIG. 4. (Color online) (a) RMS fluid velocity fluctuations u'_{rms} as a function of Φ_m. In the inset velocity fluctuations are normalized with the mean flow. (b) RMS particle density fluctuations θ'_{rms} as a function of St.

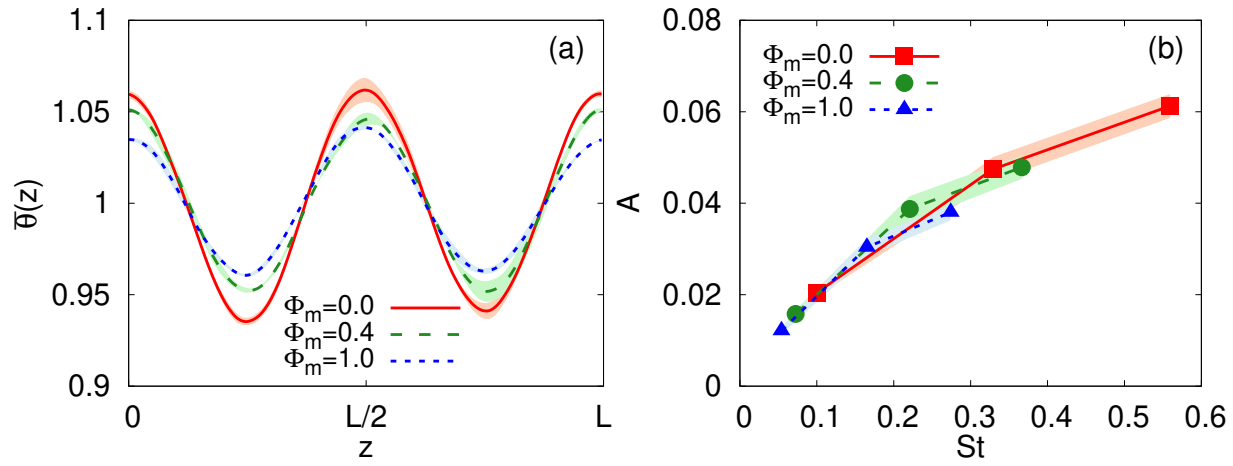

FIG. 5. (Color online) (a) Mean particle density profile $\overline{\theta}(z)$ for different values of mass loading $\Phi_m = (0.0, 0.4, 1.0)$ and fixed Stokes time $\tau = 0.58$. (b) Amplitude A of the spatial modulation of the density profile $\overline{\theta}(z) = 1 + A\cos(2Kz)$, as a function of the Stokes number St for different values of Φ_m.

In the Kolmogorov flow, the turbophoretic effect can be observed only by long time averages of the density profiles, but it is not directly visible in the instantaneous density fields. As shown in Fig. 1, the latter are characterized by filaments of clustered particles. Clustering intensity can be quantified by decomposing the particle density field as $\theta = \overline{\theta} + \theta' = 1 + A\cos(2Kz) + \theta'$. The values of the RMS density fluctuations θ'_{rms} are shown in Fig 4b. Similarly to what observed for the amplitude A of the mean density profile, we find that θ'_{rms} reduces at increasing mass loading Φ_m. Again, this is due to the reduction of turbulence at increasing Φ_m, which results in larger values for the Kolmogorov times τ_η and hence reduces the particles Stokes number $St = \tau/\tau_\eta$. Particle clustering is therefore suppressed by the mass loading.

The effects of the solid phase on the fluid can be further quantified by inspecting the equation for the local balance of fluid momentum. By averaging (1) over x, y and t, we obtain the equation

$$\partial_z \overline{u_x u_z} - \nu \partial_{zz} \overline{u_x} - F\cos(Kz) - \frac{\Phi_m}{\tau}\overline{\theta(v_x - u_x)} = 0\,, \tag{7}$$

for the mean profiles of the turbulent Reynolds stress ($\overline{u_x u_z}$), of the viscous stress ($\nu\partial_z\overline{u_x}$) of the forcing ($F\cos(Kz)$) and of the momentum exchange with the solid phase ($\frac{\Phi_m}{\tau}\overline{\theta(v_x - u_x)}$). Because of the monochromatic forcing, we can assume at first approximation a monochromatic profile for the terms in Eq (7), i.e. besides (5) we assume

$$\overline{u_x u_z} = S\sin(Kz), \qquad \overline{\theta(v_x - u_x)} = -X\cos(Kz) \tag{8}$$

where S is the amplitude of the Reynolds stress and X is the amplitude of the momentum exchange. Following Ref. [44], inserting Eqs. (5) and (8) in the momentum equation (7), yields the following

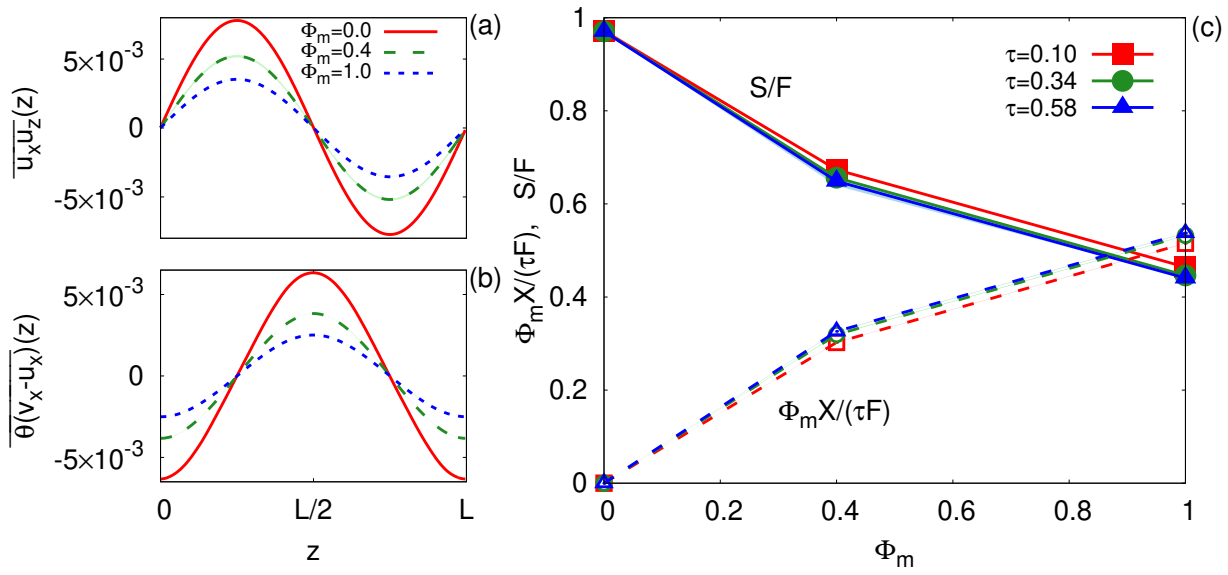

FIG. 6. (Color online) Momentum budget. Mean profile (a) of the Reynolds stress term and (b) of the momentum exchange term for different mass loadings as in label, with $\tau = 0.58$. Panel (c) shows the momentum budget for the amplitudes divided into Reynolds stress term (filled symbols) and exchange term (empty symbols), as a function of the mass loading Φ_m for different values of Stokes times as in label.

algebraic relation for the amplitudes

$$-SK - \nu K^2 U + F - \frac{\Phi_m}{\tau} X = 0\,. \tag{9}$$

In Fig. 6a-b, we show the profiles of the Reynolds stress and momentum exchange for different values of Φ_m and $\tau = 0.58$. They are very well approximated by the monochromatic functional form (8). The amplitudes of the Reynolds stress and exchange terms, normalized with the forcing amplitude F, are shown in Fig. 6c. The amplitude of the viscous term $\nu K^2 U/F$ (not shown) remains small with respect to the other terms (its effect on the total budget is only about $2-3\%$). For vanishing mass loading ($\Phi_m = 0$), the exchange term is zero and the Reynolds stress contribution is maximum, while increasing Φ_m the two terms becomes of the same order. For even larger mass loading ($\Phi_m \gtrsim 1$) the coupling term dominates over the Reynolds stress term. Notice that the dependence on τ is very weak, this is consistent with the observation that, since at leading order $\boldsymbol{v} - \boldsymbol{u} \approx -\tau D_t \boldsymbol{u}$, the amplitude of exchange term X is order τ, meaning that $\Phi_m X/\tau F$ depends upon τ only at higher orders.

The dimensionless version of the momentum budget is obtained by dividing all the terms of Eq. (9) by KU^2 and defining the friction coefficient $f = F/(KU^2)$ [44], (quantifying the ratio between the work done by the force and the kinetic energy of the mean flow) the Reynolds stress

coefficient $\sigma = S/U^2$, and the exchange coefficient $\chi = \Phi_m X/(\tau K U^2)$:

$$f = \frac{1}{Re} + \sigma + \chi \,. \tag{10}$$

In Fig. 7a, we show the friction factor f as a function of the Reynolds number. In the absence of particles ($\Phi_m = 0$) an asymptotic constant value for the friction coefficient is reached for large enough Reynolds numbers as $f = f_0 + b/Re$ (with $f_0 = 0.124$ and $b = 5.75$)[44]. Figure 7a shows that the presence of particles increases the friction coefficient, by reducing the mean velocity U. We remark that, since both f and Re depend solely on U and do not depend explicitly on the particle parameters τ and Φ_m, all the values of f obtained in the simulations at fixed F and ν lie on the curve $f = F/(\nu^2 K^3 Re^2)$. Not surprisingly, the effect is stronger for larger values of Φ_m (vanishing in the passive limit $\Phi_m = 0$). Conversely, the dependence of the friction coefficient f on the inertia is counterintuitive. One could expect that in the limit $St \to 0$ the particles become passive and they do not affect the flow, while we find that the largest friction is obtained with smaller Stokes times, in particular for large Φ_m.

We understand the non-trivial dependence on St as resulting from the combination of two effects. First, in the limit $St \to 0$ at finite mass fraction Φ_m the particles reduce the effective forcing intensity, causing an increase of the drag coefficient. Second, this increase is mitigated by the turbophoresis for particles with larger St, thus leading to values of f closer to that of the pure fluid. Let us discuss in detail these two mechanisms. As shown above (*Cfr.* Eq. (6)), in the limit of vanishing inertia $St \to 0$ the velocity field $\boldsymbol{u}$ is equal to that of a pure fluid (without particles) which satisfies the Navier-Stokes equation with rescaled forcing $\boldsymbol{f}'_{ext} = \boldsymbol{f}_{ext}/(1+\Phi_m)$ and viscosity $\nu' = \nu/(1+\Phi_m)$ [59]. The friction factor of the dusty Kolmogorov flow is therefore: $f = F/(KU^2) = (1+\Phi_m)F'/(KU^2) = (1+\Phi_m)f'$, where $f' = F'/(KU^2)$ is the friction factor of the pure fluid with rescaled Reynolds number $Re' = U/(\nu' K) = Re(1+\Phi_m)$. For $Re \gg 1$ the friction factor f' follows the asymptotic behavior $f' = f_0 + b/Re'$. This leads to an expression for the friction factor of the particle-laden flow at large Re and small St:

$$f = (1+\Phi_m) f_0 + \frac{b}{Re} \,. \tag{11}$$

This explains why we observe an increased drag f in the limit $St \to 0$ at finite Φ_m. Equating the above relation with $f = F/(\nu^2 K^3 Re^2)$ we get a prediction for Re (valid for $Re \gg 1$ and $St \ll 1$) in terms of the parameters F, K, ν, Φ_m:

$$Re = \frac{b}{2 f_0 (1+\Phi_m)} \left[\sqrt{1 + 4 \frac{f_0 (1+\Phi_m) F}{b^2 \nu^2 K^3}} - 1 \right] . \tag{12}$$

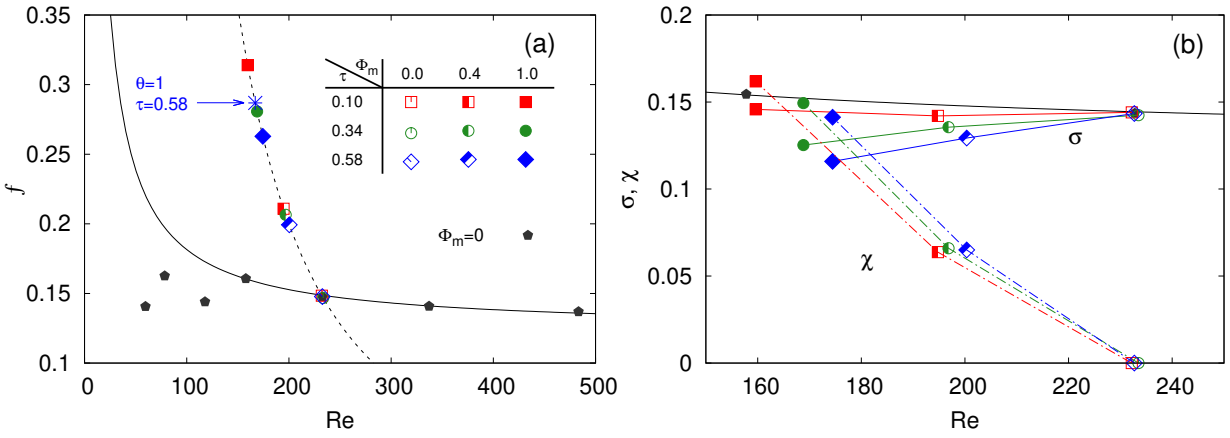

FIG. 7. (Color online) Friction and stress coefficients. (a) Friction factor f (filled symbols) as a function of Re for all the parameter configurations (Φ_m,τ) as in legend. The black pentagons are the values of f in the absence of particles ($\Phi_m = 0$) and the black continuous line is $f = f_0 + b/Re$ with $f_0 = 0.124$ and $b = 5.75$ [44]. Dashed line represents the curve $f = F/(\nu^2 K^3 Re^2)$. Blue asterisk corresponds to the simulation with imposed uniform density ($\theta = 1$) at $\Phi_m = 1$ and $\tau = 0.58$ (same parameters of run C3). (b) Stress coefficient σ (solid curves) and exchange coefficient χ (dotted curves).

The values of Re obtained in our simulations with the smallest inertia ($\tau = 0.10$) are in agreement (within 5%) with the prediction (12). The mitigation of the drag enhancement (11) that we observe at increasing inertia, is due to the turbophoresis. Since turbophoresis reduces the concentration of particles in the regions of higher turbulence intensities, it is expected to reduce, by a negative feedback, the effect of particles on the turbulent flows. Therefore the resulting friction coefficient should be closer to that of the pure fluid for particles with larger St. In order to demonstrate this point, we performed additional simulations of equations (1-2) in which the particle density field is artificially imposed to be homogeneous ($\theta \equiv 1$), thus switching off any turbophoretic effect. The result of these simulations is shown in Fig. 7a for the largest Stokes time ($\tau = 0.58$) and mass loading $\Phi_m = 1$. It is evident that, at given Φ_m and τ, the simulation with imposed uniform concentration produces a larger effect (larger friction coefficient) with respect to the fully coupled model, since it suppress the negative feedback produced by turbophoresis. Because of this effect, at fixed Φ_m, particles with larger τ, displaying a larger turbophoretic effect, cause a weaker increase of the drag coefficient than the particles with smaller τ, as observed in Figure 7.

We finally consider the behavior of the stress coefficient σ. We remark that in absence of particles ($\Phi_m = 0$), σ follows the expression $\sigma = f_0 + (b-1)/Re$ [44], inherited from the Re-dependence of the friction factor f. Increasing the mass loading $\Phi_m > 0$, σ attains values not too

far from the case $\Phi_m = 0$, but slightly shifted below. By considering points at constant τ, they appear to be disposed in lines that stray from the point at $\Phi_m = 0$ with different slopes. Increasing τ, the lines gradually deviates from the curve at $\Phi_m = 0$. Increasing the mass loading, σ decreases while χ grows, similarly to what observed for the momentum budget in Fig 6c. Although, the momentum balance indicates a drastic reduction of the Reynolds stress S, the stress coefficient σ shows a much weaker dependence on Φ_m, with only moderate variations 20% at most, with respect to the friction coefficient f, which is increased of about 110%.

V. SUMMARY AND PERSPECTIVES

In this work we have presented the results of numerical simulations of a fully Eulerian model for a two-way coupled particle-laden turbulent Kolmogorov flow at varying the inertia and mass loading of the dispersed particle phase. The peculiarity of the Kolmorogov flow is that, while it has no material boundaries, it is characterized by a well defined mean velocity profile as well as persistent regions of low and high turbulent intensity. These features are here exploited to study the active role of the particles in the phenomena of drag enhancement and turbophoresis occurring in bulk flow.

We have shown that, at increasing mass loading, the Stokes drag exerted by particles on the fluid phase induces a reduction of both the mean flow and the turbulent fluctuations. As a consequence, the presence of suspended particles reduces the Reynolds number and increases the friction coefficient, defined as the ratio between the work of the external force and the kinetic energy of the mean flow. Noteworthy, we have found that the drag enhancement is higher in the case of particles with smaller inertia which, at a first glance, appears counterintuitive because for vanishing inertia particles are expected to recover the dynamics of fluid elements. While the latter expectation is true, one must consider that the particles are heavier than the fluid. As a result, the fluid and the particles, in the limit of vanishing inertia, basically form a denser fluid. Using this simple idea, originally due to Saffman [41], we could explain the apparently counterintuitive dependence on the Stokes number in terms of an effective rescaling of the forcing amplitude caused by the increase in fluid density. The suppression of turbulent intensity at increasing mass loading causes a reduction of the turbophoresis, quantified by the amplitude of the spatial modulation in the mean particle density profile. As expected, this effect is more pronounced for particles with large inertia. Furthermore, because of their preferential migration toward regions of weaker turbulent intensity, particles with large inertia are less efficient in exerting their drag on the fluid and, therefore, they

cause a weaker drag enhancement with respect to particles with smaller inertia at equal mass loading.

It is worth comparing the effects of the particle phase in the Kolmogorov flow with those observed in channel flows. The reduction of the turbophoresis at increasing mass loading and turbulent attenuation are observed both in the Kolmogorov and channel flows [14, 48]. Drag enhancement observed in the Kolmogorov flow seems to be at odds with the observation of Ref. [19] that reported drag reduction in channel flow simulations, however, other works did not find significant variations of the mean flow [14, 15]. In general, in wall bounded flows the effects of the particles in the boundary layers might be sensitive to details and more important than those occurring in the bulk flow, in this respect the Kolmogorov flow provides a useful numerical setup to investigate the latter.

Concerning the relative importance of the mass loading and inertia, based on our numerical simulations of the particle-laden Kolmogorov flow, we found that while the inertia plays a major role in the particles' dynamics, it has a weaker influence on the properties of the flow, which are more critically dependent on the mass loading. We observed, however, that any change in the mass loading Φ_m results also in a change of the Stokes number St. Indeed, an increase in the mass loading can be achieved by (i) increasing the material density of the particle ρ_p, (ii) increasing their size a, (iii) increasing the number of particles N_p. The cases (i) and (ii) directly imply an increase of the particle response time τ, and therefore of the Stokes number. In the case (iii) τ remains unchanged, but the viscous time τ_η is affected by the reduction of turbulent fluctuations, producing again a change of St.

A variety of open questions and issues here can be addressed using the present model. First of all, remaining within the settings of the Kolmogorov flow, it would be interesting to study the effect of particles on the stability properties at the transition from the laminar to the turbulent regime, where the role of particle inertia can be important. It would also be interesting to exploit the Eulerian model here discussed for studying modifications of turbulence at small scales extending the preliminary study of Ref. [24] in two-dimensional turbulence and comparing with the results obtained with Eulerian-Lagrangian models [23, 25]. Moreover, the model can be easily modified to include gravity allowing to study sediment-laden flows [5] or particle-induced Rayleigh-Taylor instability [60].

ACKNOWLEDGMENTS

We acknowledge HPC CINECA for computing resources (INFN-CINECA Grant No. INFN19-fldturb). G.B. and S.M. acknowledges support from the Departments of Excellence grant (MIUR). A.S. acknowledges the Italian research project MODSS (Monitoring Debris Space Stereo) Grant No. ID 85-2017-14966, funded by Lazio Innova (Regione Lazio).

Appendix A: Details on numerical simulations

1. Comparison with Lagrangian scheme

In this appendix we benchmark the fully Eulerian model (1-3), in the absence of back reaction ($\Phi_m = 0$), with previous numerical results, obtained with one-way coupled inertial particles integrated with a Lagrangian scheme [39]. In particular, the latter were performed with the same parameters reported in Table I (see runs A1,B1 and C1), with grid resolution $M = 128$ and $N_p = 4 \cdot 10^5$ particles for each value of the Stokes time τ. In Fig. 8, we compare the mean particle density profiles obtained with the Eulerian model and with the Lagrangian simulations for $\tau = (0.10, 0.34, 0.58)$. As one can appreciate the two schemes are in in very good agreement.

2. Role of small-scale regularization

As discussed in Sec. III, to mitigate the possible onset of instabilities due to the formation of strong gradients in the particle density and velocity fields, Eqs. (2-3) must be regularized at small scales. To this aim, as customarily done in numerical simulations, especially when using a pseudo-spectral scheme, one can add an artificial hyperviscous term $\nu_p(-1)^{h+1}\nabla^{2h}\boldsymbol{v}$ to Eq. (2) and a hyperdiffusivity term $\kappa(-1)^{h+1}\nabla^{2h}\theta$ to Eq. (3). The power h controls the order of the hyperviscosity and diffusivity, the higher the value the more the effect of dissipation can be confined to small scales. However, it is usually convenient to consider low orders of hyperviscosity and diffusivity to avoid the phenomenon of bottleneck [61].

The results shown in Sec. IV have been obtained with a standard Laplacian term ($h = 1$) and moreover, to minimize the number of parameters, we have chosen $\nu_p = \kappa = 10^{-3}$ equal to the fluid viscosity ν. To test the impact of the chosen regularization on the presented results, we performed a few additional simulations using a higher order regularization, in particular we used $h = 2$ with $\nu_p = \kappa = 10^{-6}$. In this appendix, we show that the effect of the regularization is actually very

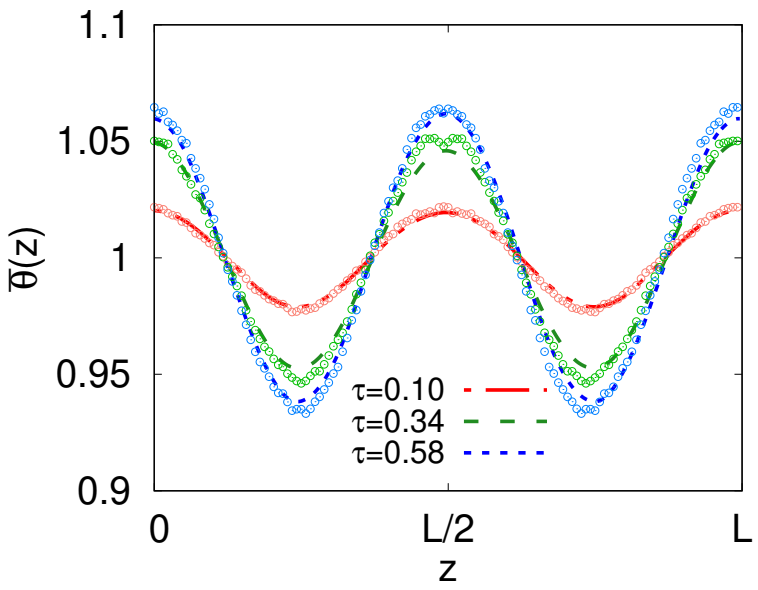

FIG. 8. (Color online) Mean particle density profile $\overline{\theta}(z)$ for different values of Stokes time (see legend) obtained with the fully Eulerian scheme with $\Phi_m = 0.0$ (dashed curves) and with the one-way coupling Lagrangian scheme of Ref.[39] (symbols). Lagrangian data have a poorer statistics with respect to Eulerian ones, therefore to decrease a bit the statistical fluctuations we exploited the symmetry with respect to $L/2$ to further average the density profile.

weak and that the results presented in Sec. IV are robust. For the sake of comparison, we have replicated two sets of simulations with the higher order regularization namely, with reference to Table I, we have fixed $\tau = 0.34$ and explored all value of Φ_m (runs B1-B3), and fixed $\Phi_m = 1.0$ for all the values of τ (runs A3, B3 and C3). To reduce the computational time, these additional runs have been performed with half the statistics of the previous ones. Therefore error bars are slightly larger than the ones considered in the viscous simulations reported in the main text.

In Figs. 9a,b we compare the mean profile $\overline{u}_x(z)$ of the longitudinal velocity for $\tau = 0.10$ and 0.58 with the largest mass loading $\Phi_m = 1.0$, obtained with the viscous and hyperviscous runs. With hyperviscosity, the profile is found to be increased by a small amount. In Figs. 9c and d we show the dependence of the mean flow amplitude U on Φ_m for $\tau = 0.34$ and on τ for $\Phi_m = 1$, respectively. In all cases the differences between the two regularization are within $4 - 6\%$, which is in the order of the statistical error for the hyperviscous simulations.

In Fig. 10 we report the analysis on the mean profile and amplitude of the Reynolds stress $\overline{u_x u_z}(z)$ for the available configurations of (Φ_m, τ). As before, with hyperviscosity we found a (very) weak enhancement of the Reynolds stress amplitude. However, in all cases the effect is very

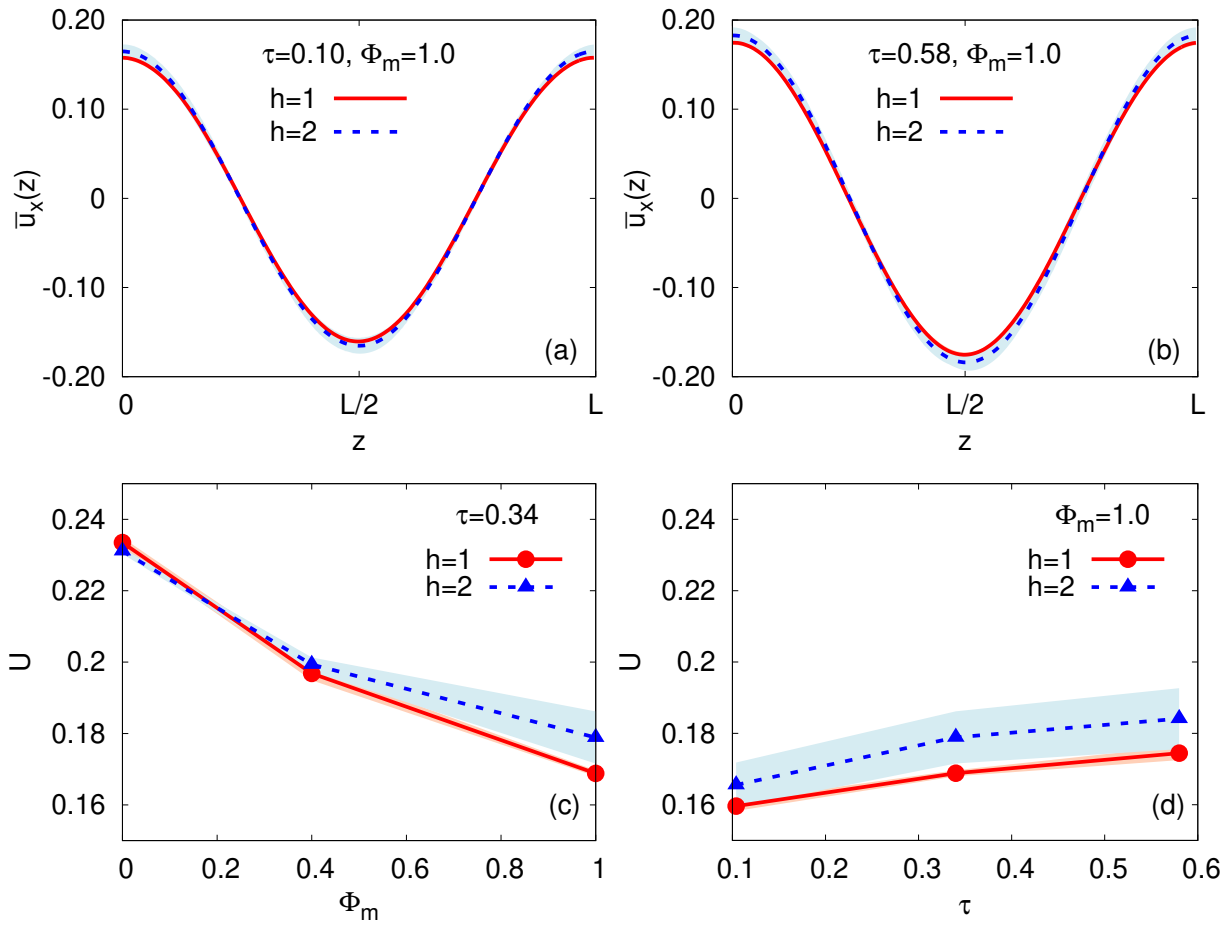

FIG. 9. (Color online) Effect of the order of the dissipative regularization ($h = 1$ and $h = 2$) on the profile of the mean longitudinal velocity: (a) and (b) $\overline{u}_x(z)$ vs z for $\Phi_m = 1$ with $\tau = 0.10$ and 0.58, respectively; (c) Amplitude of the mean flow U as a function of Φ_m for fixed $\tau = 0.34$; (c) same of (b) as a function of τ for fixed $\Phi_m = 1.0$. Parameters $\nu_p = \kappa = 10^{-6}$ for $h = 2$, for simulations with $h = 1$ see Table I.

small and nearly negligible, with relative discrepancies between $2 - 6\%$, which is in the order of statistical error for the hyperviscous simulations.

In conclusion, the results discussed in Sec. IV are robust and basically independent of the regularization scheme.

[1] N. J. Balmforth and A. Provenzale, *Geomorphological fluid mechanics*, Vol. 582 (Springer Science & Business Media, 2001).

[2] R. A. Shaw, "Particle-turbulence interactions in atmospheric clouds," Annu. Rev. Fluid Mech. **35**, 183–227 (2003).

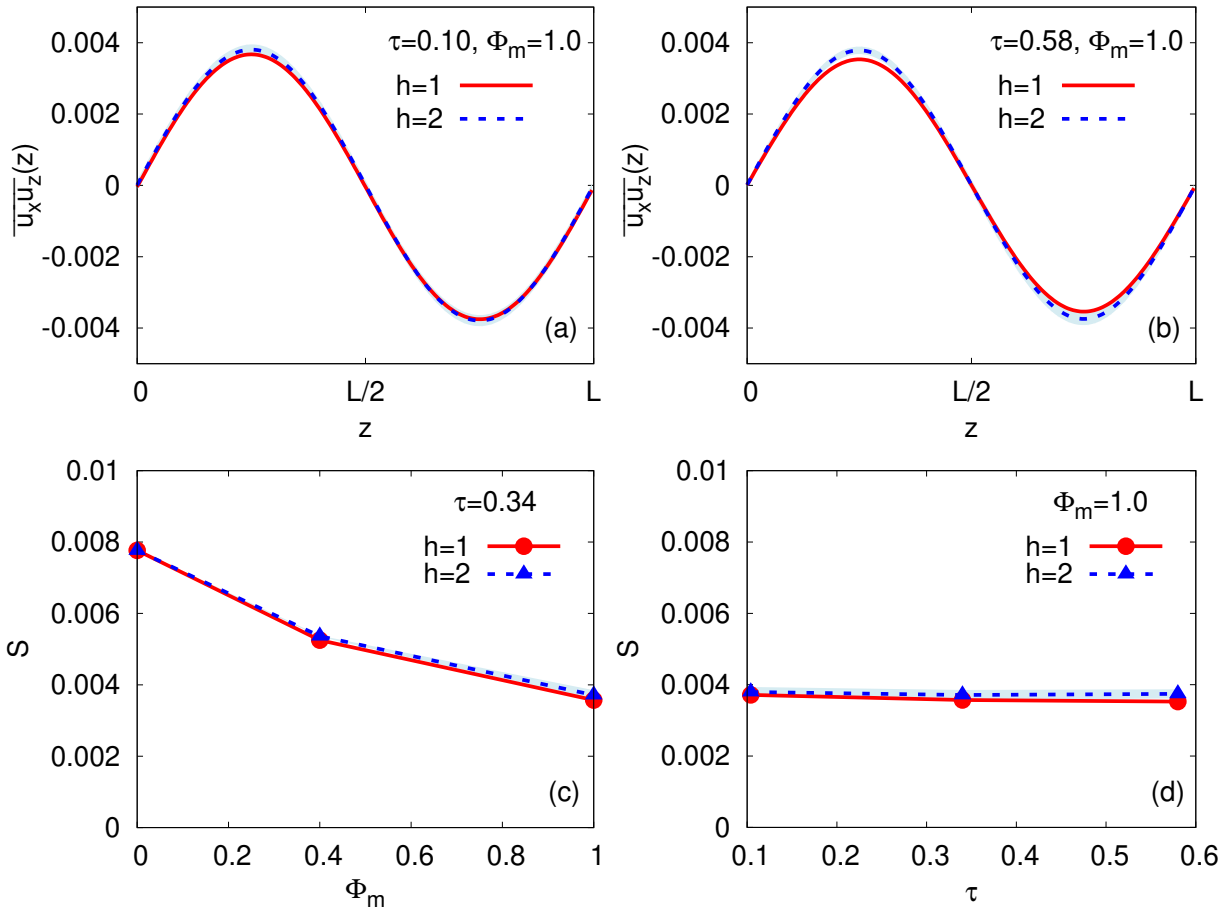

FIG. 10. (Color online) Effect of the order of the dissipative regularization ($h = 1$ and $h = 2$) on the profile of the Reynolds stress $\overline{u_x u_z}(z)$: (a) and (b) $\overline{u_x u_z}(z)$ vs z for $\Phi_m = 1$ with $\tau = 0.10$ and 0.58, respectively; (c) Amplitude of the Reynolds stress S as a function of Φ_m for fixed $\tau = 0.34$; (c) same of (b) as a function of τ for fixed $\Phi_m = 1.0$. Parameters $\nu_p = \kappa = 10^{-6}$ for $h = 2$, for simulations with $h = 1$ see Table I.

[3] A. Celani, G. Falkovich, A. Mazzino, and A. Seminara, "Droplet condensation in turbulent flows," Europhys. Lett. **70**, 775 (2005).

[4] F. Necker, C. Härtel, L. Kleiser, and E. Meiburg, "Mixing and dissipation in particle-driven gravity currents," J. Fluid Mech. **545**, 339–372 (2005).

[5] P. Burns and E. Meiburg, "Sediment-laden fresh water above salt water: nonlinear simulations," J. Fluid Mech. **762**, 156–195 (2015).

[6] D. Bercovici and C. Michaut, "Two-phase dynamics of volcanic eruptions: compaction, compression and the conditions for choking," Geophys. J. Int **182**, 843–864 (2010).

[7] P. J. Armitage, *Astrophysics of Planet Formation* (Cambridge University Press, 2010).

[8] P. J. Armitage, "Dynamics of protoplanetary disks," Annu. Rev. Astron. Astrophys. **49**, 195 (2011).

[9] H. Homann, T. Guillot, J. Bec, C. W. Ormel, S. Ida, and P. Tanga, "Effect of turbulence on collisions

of dust particles with planetesimals in protoplanetary disks," Astron. Astrophys **589**, A129 (2016).

[10] I. Lashgari, F. Picano, W.-P. Breugem, and L. Brandt, "Laminar, turbulent, and inertial shear-thickening regimes in channel flow of neutrally buoyant particle suspensions," Phys. Rev. Lett. **113**, 254502 (2014).

[11] H. T. Bi, N. Ellis, I. A. Abba, and J. R. Grace, "A state-of-the-art review of gas–solid turbulent fluidization," Chem. Eng. Sci. **55**, 4789–4825 (2000).

[12] S. Balachandar and J. K. Eaton, "Turbulent dispersed multiphase flow," Annu. Rev. Fluid Mech. **42**, 111–133 (2010).

[13] R. A. Gore and C. T. Crowe, "Effect of particle size on modulating turbulent intensity," Int. J. Multiph. Flow **15**, 279–285 (1989).

[14] J. K. Eaton, "Two-way coupled turbulence simulations of gas-particle flows using point-particle tracking," Int. J. Multiph. Flow **35**, 792–800 (2009).

[15] J. D. Kulick, J. R. Fessler, and J. K. Eaton, "Particle response and turbulence modification in fully developed channel flow," J. Fluid Mech. **277**, 109–134 (1994).

[16] R. Monchaux and A. Dejoan, "Settling velocity and preferential concentration of heavy particles under two-way coupling effects in homogeneous turbulence," Phys. Rev. Fluids **2**, 104302 (2017).

[17] M. H. Kasbaoui, "Turbulence modulation by settling inertial aerosols in Eulerian-Eulerian and Eulerian-Lagrangian simulations of homogeneously sheared turbulence," Phys. Rev. Fluids **4**, 124308 (2019).

[18] P. Muramulla, A. Tyagi, P. S. Goswami, and V. Kumaran, "Disruption of turbulence due to particle loading in a dilute gas–particle suspension," J. Fluid Mech. **889**, A28 (2020).

[19] L. H. Zhao, H. I. Andersson, and J. J. J. Gillissen, "Turbulence modulation and drag reduction by spherical particles," Phys. Fluids **22**, 081702 (2010).

[20] D. Li, K. Luo, Z. Wang, W. Xiao, and J. Fan, "Drag enhancement and turbulence attenuation by small solid particles in an unstably stratified turbulent boundary layer," Phys. Fluids **31**, 063303 (2019).

[21] M. N. Ardekani, P. Costa, W-P. Breugem, F. Picano, and L. Brandt, "Drag reduction in turbulent channel flow laden with finite-size oblate spheroids," J. Fluid Mech. **816**, 43–70 (2017).

[22] W. Fornari, A. Formenti, F. Picano, and L. Brandt, "The effect of particle density in turbulent channel flow laden with finite size particles in semi-dilute conditions," Phys. Fluids **28**, 033301 (2016).

[23] P. Gualtieri, F. Battista, and C. M. Casciola, "Turbulence modulation in heavy-loaded suspensions of tiny particles," Phys. Rev. Fluids **2**, 034304 (2017).

[24] J. Bec, F. Laenen, and S. Musacchio, "Dusty turbulence," arXiv preprint arXiv:1702.06773 (2017).

[25] V. Pandey, P. Perlekar, and D. Mitra, "Clustering and energy spectra in two-dimensional dusty gas turbulence," Phys. Rev. E **100**, 013114 (2019).

[26] E. Balkovsky, G. Falkovich, and A. Fouxon, "Intermittent distribution of inertial particles in turbulent flows," Phys. Rev. Lett. **86**, 2790 (2001).

[27] J. Bec, "Fractal clustering of inertial particles in random flows," Phys. Fluids **15**, L81–L84 (2003).

[28] J. Bec, L. Biferale, M. Cencini, A. Lanotte, S. Musacchio, and F. Toschi, "Heavy particle concentration

in turbulence at dissipative and inertial scales," Phys. Rev. Lett. **98**, 084502 (2007).

[29] M. W. Reeks, "The transport of discrete particles in inhomogeneous turbulence," J. Aerosol Sci. **14**, 729–739 (1983).

[30] S. Belan, I. Fouxon, and G. Falkovich, "Localization-delocalization transitions in turbophoresis of inertial particles," Phys. Rev. Lett. **112**, 234502 (2014).

[31] G. A. Sehmel, "Particle deposition from turbulent air flow," J. Geophys. Res. **75**, 1766–1781 (1970).

[32] M. Caporaloni, F. Tampieri, F. Trombetti, and O. Vittori, "Transfer of particles in nonisotropic air turbulence," J. Atmos. Sci. **32**, 565–568 (1975).

[33] J. W. Brooke, K. Kontomaris, T. J. Hanratty, and J. B. McLaughlin, "Turbulent deposition and trapping of aerosols at a wall," Phys. Fluids A **4**, 825–834 (1992).

[34] C. Marchioli and A. Soldati, "Mechanisms for particle transfer and segregation in a turbulent boundary layer," J. Fluid Mech. **468**, 283–315 (2002).

[35] G. Sardina, P. Schlatter, L. Brandt, F. Picano, and C. M. Casciola, "Wall accumulation and spatial localization in particle-laden wall flows," J. Fluid Mech. **699**, 50–78 (2012).

[36] F. Picano, G. Sardina, and C. M. Casciola, "Spatial development of particle-laden turbulent pipe flow," Phys. Fluids **21**, 093305 (2009).

[37] D. WI. Rouson and J. K. Eaton, "On the preferential concentration of solid particles in turbulent channel flow," J. Fluid Mech. **428**, 149–169 (2001).

[38] J. Bec, H. Homann, and G. Krstulovic, "Clustering, fronts, and heat transfer in turbulent suspensions of heavy particles," Phys. Rev. Lett. **112**, 234503 (2014).

[39] F. De Lillo, M. Cencini, S. Musacchio, and G. Boffetta, "Clustering and turbophoresis in a shear flow without walls," Phys. Fluids **28**, 035104 (2016).

[40] D. Mitra, N. E. L. Haugen, and I. Rogachevskii, "Turbophoresis in forced inhomogeneous turbulence," Europ. Phys. J. Plus **133**, 35 (2018).

[41] P. G. Saffman, "On the stability of laminar flow of a dusty gas," J. Fluid Mech. **13**, 120–128 (1962).

[42] G. I. Sivashinsky, "Weak turbulence in periodic flows," Physica D **17**, 243–255 (1985).

[43] H. Garg, E. Calzavarini, G. Mompean, and S. Berti, "Particle-laden two-dimensional elastic turbulence," Europ. Phys. J. E **41**, 115 (2018).

[44] S. Musacchio and G. Boffetta, "Turbulent channel without boundaries: The periodic Kolmogorov flow," Phys. Rev. E **89**, 023004 (2014).

[45] G. Boffetta, A. Celani, and A. Mazzino, "Drag reduction in the turbulent Kolmogorov flow," Phys. Rev. E **71**, 036307 (2005).

[46] E.L.C.VIM. Plan, S. Musacchio, and D. Vincenzi, "Emergence of chaos in a viscous solution of rods," Phys. Rev. E **96**, 053108 (2017).

[47] S. Olivieri, A. Akoush, L. Brandt, M. E. Rosti, and A. Mazzino, "Turbulence in a network of rigid fibers," Phys. Rev. Fluids **5**, 074502 (2020).

[48] D. G. E. Grigoriadis and B. J. Geurts, "Reduced turbophoresis in two-way coupled particle-laden flows,"

in *Direct and Large-Eddy Simulation VIII* (Springer, 2011) pp. 207–212.

[49] A. N. Youdin and J. Goodman, "Streaming instabilities in protoplanetary disks," Astrophys. J. **620**, 459 (2005).

[50] Daniel Carrera, Uma Gorti, Anders Johansen, and Melvyn B Davies, "Planetesimal formation by the streaming instability in a photoevaporating disk," Astrophys. J. **839**, 16 (2017).

[51] S. Elghobashi, "On predicting particle-laden turbulent flows," App. Sci. Res. **52**, 309–329 (1994).

[52] J. Bec, L. Biferale, M. Cencini, A. Lanotte, and F. Toschi, "Intermittency in the velocity distribution of heavy particles in turbulence," J. Fluid Mech. **646**, 527–536 (2010).

[53] M. Wilkinson and B. Mehlig, "Caustics in turbulent aerosols," Europhys. Lett. **71**, 186 (2005).

[54] G. Falkovich, A. Fouxon, and M. G. Stepanov, "Acceleration of rain initiation by cloud turbulence," Nature **419**, 151–154 (2002).

[55] M. Wilkinson, B. Mehlig, and V. Bezuglyy, "Caustic activation of rain showers," Phys. Rev. Lett. **97**, 048501 (2006).

[56] G. Boffetta, A. Celani, F. De Lillo, and S. Musacchio, "The Eulerian description of dilute collisionless suspension," Europhys. Lett. **78**, 14001 (2007).

[57] L. D. Meshalkin and Ia. G. Sinai, "Investigation of the stability of a stationary solution of a system of equations for the plane movement of an incompressible viscous liquid," J. Appl. Math. Mech **25**, 1700–1705 (1961).

[58] For $\Phi_m > 0$ deviations from the monochromatic form can appear because of the exchange term $\overline{\theta(v-u)}$. Expanding the density field as $\theta = 1+A\cos(2Kz)+o(A)$ in terms of the small amplitude A of the density profile, the exchange term is, at leading order, proportional to the velocity difference $\overline{(v-u)}$, which gives a monochromatic velocity profile. Deviations from the monochromatic velocity profile appears only at higher order in A.

[59] At high Re, the rescaling of the viscosity is negligible in the momentum balance, as confirmed by the data in Fig. 3.

[60] Y. Chou and Y-C. Shao, "Numerical study of particle-induced Rayleigh-Taylor instability: Effects of particle settling and entrainment," Phys. Fluids **28**, 043302 (2016).

[61] U. Frisch, S. Kurien, R. Pandit, W. Pauls, S. S. Ray, A. Wirth, and J.-Z. Zhu, "Hyperviscosity, galerkin truncation, and bottlenecks in turbulence," Phys. Rev. Lett. **101**, 144501 (2008).